Chapter 4
Optical Magneto-Spectroscopy of Graphene-Based Systems

C. Faugeras, M. Orlita, and M. Potemski

Abstract Recent results of magneto-absorption and Raman scattering studies of different graphene based systems are reviewed. The potential of these techniques to derive the band structure, scattering efficiency and effects of interactions is discussed in reference to studies of two representative allotropes of sp^2-bonded carbon: graphene and graphite.

4.1 Introduction

Graphene and its layered structures including graphite are usually classified as zero-bandgap semiconductors and/or semimetals [1, 2], and most naturally their properties are probed with electric conductivity measurements [3]. Indeed, our very first knowledge on graphite is that it is a strongly anisotropic (three dimensional) conductor [4] whereas the observation of the peculiar sequence of quantum Hall states (half-integer quantum Hall effect) is a fingerprint of the characteristic (two-dimensional) electronic states of graphene [5, 6]. What could be at first sight surprising is that optical spectroscopy has played and continues to play an important role in the research on graphene-based systems [7, 8]. Moreover, optical properties can also be decisive for a number of anticipated applications of graphitic layers, when, for example, they are used as saturable absorbers [9, 10], transparent conducting electrodes [11, 12] or plasmonic devices [13]. Notably, optical properties of graphene were a key ingredient to "see" the monolayer of carbon atoms deposited on Si/SiO_2 substrates through an optical microscope [14–18]—this was one of the unquestionable milestones in the development of the graphene oriented research. Optical spectroscopy of graphene based systems has developed today into a large area of research with many different directions. Raman scattering of phonons is one of the primary characterization tools of graphene materials [19–21] and also provides the relevant information on electron-phonon interaction in these materials [22–24]. Optical absorption is studied in a wide spectral range from far-infrared to

C. Faugeras · M. Orlita · M. Potemski (✉)
Laboratoire National des Champs Magnétiques Intenses, CNRS-UJF-UPS-INSA, 25, avenue des Martyrs, 38042 Grenoble, France
e-mail: marek.potemski@grenoble.cnrs.fr

H. Aoki, M.S. Dresselhaus (eds.), *Physics of Graphene*, NanoScience and Technology,
DOI 10.1007/978-3-319-02633-6_4,

the UV range. The experiments allow us to conclude about the characteristic doping (Drude-like free carrier absorption in the limit of low frequencies) and the specific band structure of the system studied (interband transitions in the infrared spectral range) [25]. More challenging are perhaps: the intriguing frequency independent (and given only by universal constants) optical absorption of graphene in a wide spectral range [26–28], the excitonic effects at high energies (related to van Hove singularities) [29–31] and possible modifications of the low frequency absorption response by electron-electron interactions (enhanced/suppressed Drude peak, plasmons) [32–35]. A large number of optical experiments are devoted to the studies of the dynamics of photo-excited carriers in graphene [36–45], which are closely related to possible application of graphene in optical devices. Interesting physics and also potential applications may follow the recent interest in the photo-conductivity response of graphene structures.

Optical spectroscopy appears to be a particularly forceful experimental tool to study electronic properties when it is combined with the application of magnetic fields. Primarily, this is because the application of a magnetic field significantly changes the character of the motion of a charge carrier (cyclotron motion) and/or induces a considerable modulation of the density of electronic states, including the appearance of discrete (and highly degenerate) Landau levels in the case of two-dimensional systems. When a magnetic field (B) is applied, the optical response becomes richer in resonances which notably can be tuned with the field strength. Very roughly speaking, the energies $E_n(B)$ of Landau levels (and in consequence the energies of cyclotron resonance and/or inter Landau level excitations) trace the dispersion relations $E(k)$ of the electronic states, following the approximate conjecture that $E_n(B) \propto E(k_n) = E(\frac{\sqrt{n}}{l_B})$, where n is an integer and $l_B = \sqrt{\frac{\hbar}{eB}}$ denotes the (characteristic) magnetic length. The Landau level spacing which, for example, scales as $B \cdot n$ is characteristic for parabolic bands whereas linear bands imply the $\sqrt{B \cdot n}$ scaling. Hence, Landau level spectroscopy provides, first of all, information about the band structure of the studied system. On the other hand, the analysis of the broadening of the magneto-resonances is often a relevant source of information about the efficiency of carrier scattering. The simple fact of observing the cyclotron resonance (at frequency ω_c and magnetic field B_0) already implies some estimate of the carrier scattering time (τ) and/or mobility (μ): $\omega_c \cdot \tau = \mu \cdot B_0 > 1$. Optical magneto spectroscopy is also a valuable tool to study the physics of interactions. This certainly concerns the electron-phonon interaction because of the convenient possibility to tune the electronic excitations (with the magnetic field) across the characteristic phonon energies. Furthermore, the magneto-optical response of an electronic system (in particular of a two-dimensional one) may also imply the effects of electron-electron interactions. One must however admit that those latter effects are most often hardly seen in the experiment. This can be understood when probing the electronic states with parabolic dispersion relations (optically active, zero momentum excitation are insensitive to electron-electron interactions) but remains surprising in the case of two-dimensional systems with linear bands.

As for the methods of optical magneto-spectroscopy, the typical magneto-absorption, essentially in the far-infrared and microwave spectral range, is the most

common technique applied to study graphene based materials. Pioneer magneto-absorption measurements provided a relevant input to understand the electronic properties of graphite already more than a half century ago [46, 47]. As shown in this paper, those measurements have been more recently applied to many other graphene based structures, providing valuable information on their band structure and on the scattering efficiency as well as some input to the physics of interactions in these systems. The methods of optical magneto-spectroscopy are complementary to other, for example, electric transport techniques widely applied to study graphene based materials. Optics appears to be obviously advantageous when structures cannot be contacted/gated or when they consist of multilayered material with different components (which can be spectrally resolved). So far, infrared magneto-spectroscopy studies have been mostly limited to simple absorption type measurements [7]. More information (particularly on the physics of the quantum Hall effect) can be deduced when investigating the response of graphene with Faraday rotation experiments [48], but only very first experiments towards this direction have been announced so far [49, 50]. A clear drawback of magneto-spectroscopy at long wavelengths is that it is hardly applied to small graphene flakes and that the polarization-resolved optics is also not very easy to handle in this spectral range. The methods of Raman scattering, in a visible optical range, becomes then advantageous. Notably, these are only very recent magneto-Raman scattering experiments [51, 52] which show the possibility to trace the electronic response (inter Landau level excitations) in graphene based structures [53, 54] using this technique. The results of these relatively new experiments are largely discussed here. High quality of the electronic system seems to be essential for tracing the electronic response in magneto-Raman scattering experiments but we believe this will be possible in case of many different graphene systems in the future.

The intention of this report is to present what can be learned from optical magneto-spectroscopy studies of graphene based materials. Our main focuses are two material systems: graphene (and/or graphene-like structures) and bulk graphite; and the results of two types of experiments: of the magneto-absorption at long wavelength (far-infrared and microwave range) and of the magneto-Raman scattering. Section 4.2 is devoted to graphene with the subsequent subsections focused on the aspects of the band structure, carrier scattering and the effects of interactions (essentially electron-phonon). Section 4.4, devoted to graphite, has a similar structure. Bilayer graphene is only briefly discussed (Sect. 4.3) since only few magneto-optical investigations of these system has been reported so far.

4.2 Magneto-Spectroscopy of Graphene

4.2.1 Classical Cyclotron Resonance of Dirac Fermions

Cyclotron motion of charge carriers and the related cyclotron resonance (absorption of light at the cyclotron frequency ω_c) is primarily a classical effect, probably the

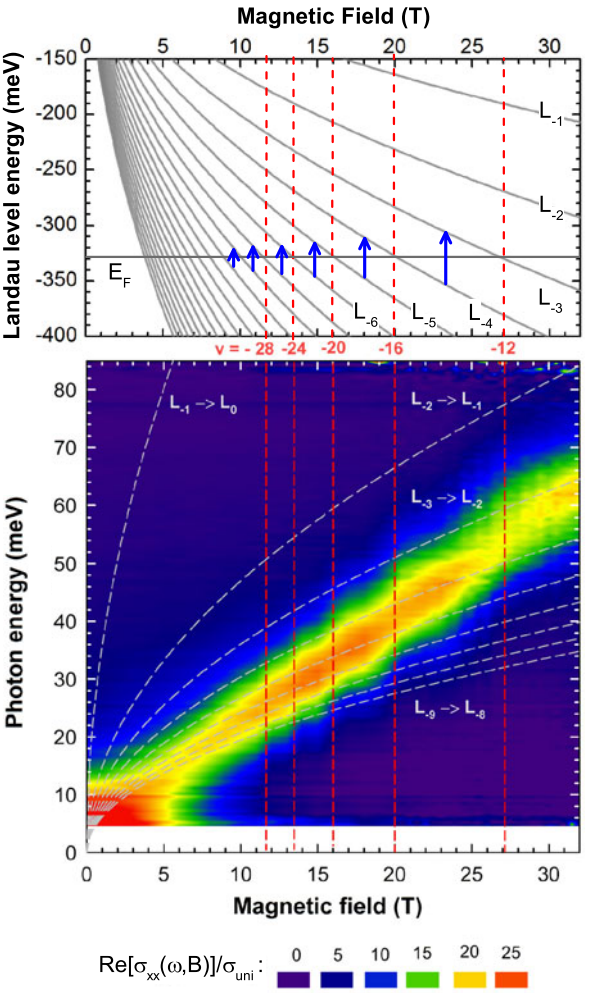

Fig. 4.1 *Upper panel*: Landau level fan chart with schematically-shown cyclotron resonance transitions in the quantum regime. *Lower panel*: A color plot of the real part of the experimentally determined longitudinal optical conductivity $\sigma_{xx}(\omega, B)$. The *dashed lines* correspond to transitions between adjacent (hole) Landau levels in graphene, $L_{-m} \rightarrow L_{-m+1}$. In both panels, a Fermi velocity $v_F = 0.99 \times 10^6$ m/s was considered to draw theoretical lines. Taken from Ref. [35]

most representative for magneto-optical spectroscopy studies. Importantly, the cyclotron motion is not only characteristic for a conventional charged (e) particle with mass m, which precesses with the frequency of $\omega_c = eB/m$, but also for massless Dirac fermions. The solution of the classical equation of motion for a charged particle with energy ε that depends linearly on momentum p ($\varepsilon = v_F p$), also results in the cyclotron motion but with a frequency $\omega_c = eB/(|\varepsilon|/v_F^2)$, in which one easily identifies the energy dependent mass $m = |\varepsilon|/v_F^2$. This latter expression, equivalent to the Einstein relation between mass and energy, invokes the relativistic-like character of electronic states in graphene. Perhaps surprisingly, the classical regime of the cyclotron resonance of graphene has been evidenced only recently [55]. This classical regime, characteristic of the linear in B cyclotron resonance (CR) absorption at low magnetic fields is illustrated in Fig. 4.1 with recent results obtained on

highly p-doped quasi-free standing epitaxial graphene on the silicon-terminated surface of silicon carbide. If the 2D translational symmetry of (highly-doped) graphene is broken either by the presence of specific disorder, or artificially, by lithographical patterning, effects of classical plasma dominate the optical response—CR is replaced by magneto-plasmon resonances [56, 57].

It is worth noticing that the classical CR absorption is accompanied by a Faraday-rotation effect, as demonstrated by Crassee et al. [49]. At higher fields, the quantum regime of CR is approached [35] and CR gains the characteristic $\sqrt{B}$ dependence, see Fig. 4.1. The related Faraday rotation is expected to be quantized in units of the fine structure constant [48], as indeed indicated in recent experiments [50]. Such a quantum regime of the magneto-optical response of graphene is described in the following section.

4.2.2 Magneto-Optical Response of Graphene: Quantum Regime

The specific electronic structure of graphene, namely the vanishing cyclotron mass in the vicinity of the Dirac point, implies a rather large spacing between Landau levels. A fully quantum-mechanical approach thus becomes necessary even in relatively low magnetic fields, if we deal with a weakly doped graphene specimen. In a quantum-mechanical picture, the application of the magnetic field B perpendicular to the graphene plane transforms the continuous electronic spectrum into discrete and highly degenerate Landau levels (LLs) [58]:

$$E_n = \mathrm{sign}(n) v_F \sqrt{2|e|\hbar B|n|} = \mathrm{sign}(n) E_1 \sqrt{|n|}, \quad n = 0, \pm 1, \pm 2 \ldots \tag{4.1}$$

which positions are defined by a single parameter, the Fermi velocity v_F ($E_1 = v_F\sqrt{2\hbar|e|B}$). The degeneracy of each Landau level is $\zeta(B) = g_v g_s |eB|/h$, where we take into account both spin g_s and valley g_v degeneracies. This LL spectrum consists of electron levels ($n > 0$), hole levels ($n < 0$) and a zeroth LL ($n = 0$) which is shared by both hole and electron types of carriers and which is responsible for the unusual sequence of the quantum Hall effect in graphene [5, 6]. We also immediately see that LLs in graphene are non-equidistant, they evolve as $\sqrt{B}$, see Fig. 4.2a, and both the spacing and the field dependence, can be understood as a consequence of the extreme non-parabolicity (in fact linearity) of the bands. The unusual $\sqrt{B}$-dependence of LLs is responsible for the surprising sensitivity of graphene electronic states to a magnetic field. Experimentally, well-defined LLs have been observed in this system down to 1 mT and almost up to the temperature of liquid nitrogen [59]. It might be realistic that Landau level quantization in pure graphene could also be observable in the magnetic field of the Earth ($B_{\mathrm{Earth}} \sim 10^{-5}$ T), which is unique for a condensed-matter system.

Interaction of light with graphene in a quantizing magnetic field has been explored extensively both theoretically and experimentally over the few past years [53, 59–73]. Graphene exhibits a relatively rich (multi-mode) magneto-optical response, where the energies of individual resonances correspond to the individual

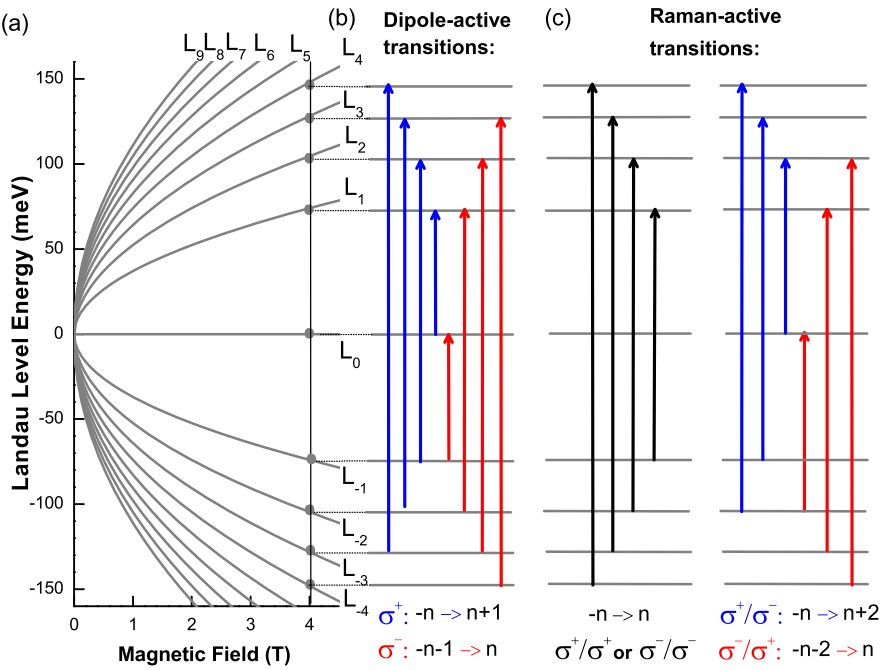

Fig. 4.2 (**a**) Characteristic $\sqrt{B}$-dependence of LLs in graphene shown for a few low-index levels. Dipole-allowed and Raman-active (Stokes branch) inter-LL transitions in undoped graphene are shown in parts (**b**) and (**c**), respectively

inter-LL transitions and scale as $\sqrt{B}$. This unique property of the Landau level spectrum is thus preserved in the magneto-optical response.

All dipole-allowed inter-LL transitions in graphene follow the selection rules $|n| \rightarrow |n| + 1$ and $|n| \rightarrow |n| - 1$, which are active in the σ^+ and σ^- polarizations of the incoming light [67, 69], respectively. These dipole-active transitions can be divided into three groups ($j \geq 1$): Inter-band resonances $L_{-j} \rightarrow L_{j+1}$ and $L_{-j-1} \rightarrow L_j$ at an energy $E_1(\sqrt{j+1} + \sqrt{j})$, intra-band resonances $L_j \rightarrow L_{j+1}$ and $L_{-j-1} \rightarrow L_{-j}$ at an energy $E_1(\sqrt{j+1} - \sqrt{j})$, and the mixed $L_{-1(0)} \rightarrow L_{0(1)}$ resonance, involving the $n = 0$ LL, which has an energy of E_1. Typical magneto-transmission data taken on quasi-neutral sheets of multilayer epitaxial graphene are shown in Fig. 4.3. The spectra are in this particular case dominated by the mixed mode $L_{-1(0)} \rightarrow L_{0(1)}$; nevertheless, a series of interband inter-LL resonances is also well resolved. Experimentally, this behaviour has been observed in multilayer epitaxial graphene with a characteristic rotational stacking of adjacent layers [62, 66, 67, 70, 71] and also in exfoliated graphene specimens [64, 68].

The intra-band transitions appear at low energies and are followed by inter-band resonances at higher energies. There is however no distinct separation in energy scale between these two types of transitions, which is in contrast to the case of conventional 2D systems based on gapped semiconductors, but somehow similar to the case of narrow-gap II/VI compound structures [74–77]. Nevertheless, in graphene,

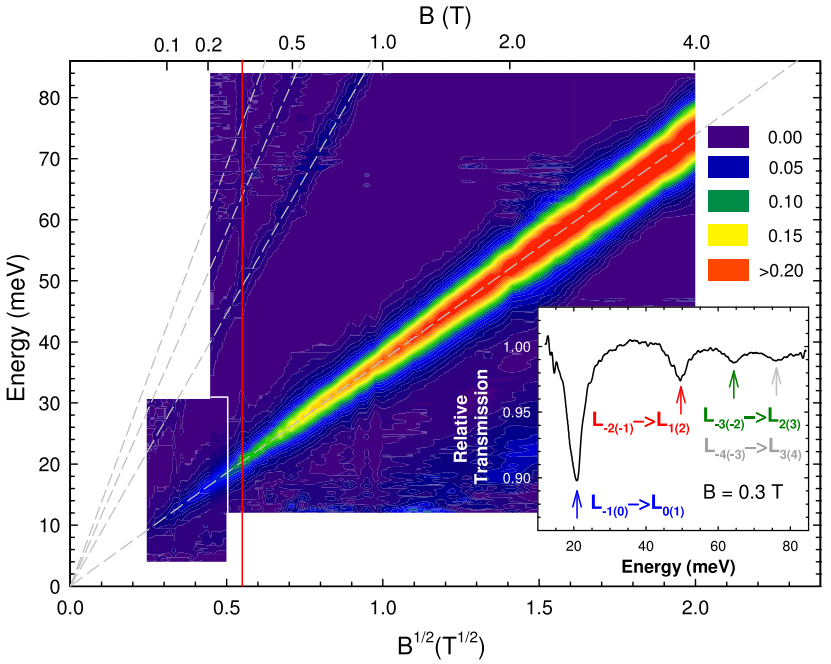

Fig. 4.3 Far infrared transmission $\mathcal{T}$ plotted as $-\ln\mathcal{T}$ as a function of the magnetic field at $T = 2.0$ K. The *dashed lines* denote the expected transitions for $v_F = 1.02 \times 10^6$ m s^{-1}. The *inset* shows the transmission spectrum at $B = 0.3$ T. Copyright (2008) by The American Physical Society

we deal with only one type of atomic orbital, and therefore both intra- and inter-band transitions follow similar selection rules: namely, the modulus of the LL index is changed by 1. This is again in contrast to the case of conventional 2D systems, made for instance from GaAs, for which the inter-band transitions conserve the LL index and their dipole moment is due to different s- and p-orbitals in the conduction and valence bands, respectively. Owing to the electron-hole symmetry of the graphene band structure, two different inter-band resonances, such as, for example $L_{-2} \rightarrow L_3$ and $L_{-3} \rightarrow L_2$ in Fig. 4.2b, may appear at the same energy. Such energy degenerated transitions are, however, active in opposite circular polarizations of light. At low temperatures one may expect at most two different intra-band transitions, but a series of inter-band transitions. The situation is even more complex at higher temperatures, when the thermal spreading of the Fermi distribution exceeds the separation between Landau levels. The intra-band absorption (CR) may then also reveal a multi-mode character, due to partial occupation of a few non-equidistant LLs curve depicts the thermal activation of $L_0 \rightarrow L_1$. Such a multi-mode intra-band absorption spectrum, with an envelop that corresponds, *nota bene*, to the classical cyclotron resonance, discussed at the beginning of this section, was recently observed in graphene (on the surface of bulk graphite) by Neugebauer et al. [59].

Inter-LL excitations visible in Raman scattering experiments follow different selection rules [53]. To indicate the different polarization configurations, we use the

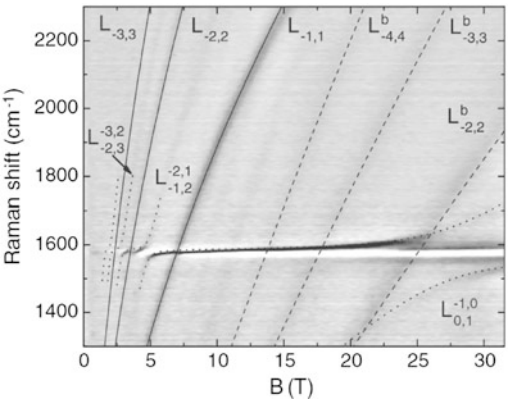

Fig. 4.4 Grey scale plot of the unpolarized scattered intensity as a function of the magnetic field measured on natural graphite specimens. The $B = 0$ spectrum has been subtracted from each spectra. Three different types of excitations are observed: *Solid* and *dotted lines* correspond to interband inter-LL excitations in decoupled graphene flakes on graphite. The latter are coupled with E_{2g} phonon line resulting in characteristic avoided crossing behavior. *Dashed lines* correspond to interband inter-LL excitations at the K point of bulk graphite. For details see Refs. [79] and [51]. Copyright (2011) by The American Physical Society

notation $\sigma_{Excitation}/\sigma_{Collection}$ where $\sigma_{Excitation}$ is the circular polarization of the excitation photon and $\sigma_{Collection}$ the one of the collected photon. The dominant contribution to the Stokes component of the Raman scattering spectrum is provided by transitions symmetric with respect to the $n = 0$ LL, $-n \rightarrow n$ with $n > 0$, see Fig. 4.2, that are visible in the so-called co-circular configuration, in which the in-coming and out-going photons keep the same circular polarization (σ^-/σ^- or σ^+/σ^+). These excitations have been detected in the Raman scattering spectra of graphene-like locations on the surface of bulk graphite and represent probably the first purely electronic excitation in graphene observed in Raman scattering experiments (see Fig. 4.4). It is worth noticing that more recently, a purely electronic Raman scattering signal has been also found in metallic carbon nanotubes [78]. The other (relatively weak) contribution, predicted to be active in the cross-circular polarization [53] (σ^+/σ^- and σ^+/σ^-) and following the selection rule $-n \rightarrow n + 2$ and $-n - 2 \rightarrow n$, respectively, see Fig. 4.2c, has not yet been observed experimentally.

4.2.3 Landau Level Fan Charts and Fermi Velocity

A clear illustration of the characteristic $\sqrt{|Bn|}$ scaling of Landau levels, in fact equivalent to the observation of linear dispersion relations of carriers, has been the first important feat of the Landau level spectroscopy of graphene systems [62]. Sadowski et al. [62] observed a practically perfectly $\sqrt{|Bn|}$-scaled Landau level fan chart in multilayer epitaxial graphene (MEG) structures and extracted the only scaling parameter—the Fermi velocity, $v_F = 1.03 \times 10^6$ m s^{-1}. Jiang et al. [64]

and subsequently Deacon et al. [68] found somehow higher values $v_F \approx 1.1 \times 10^6$ m s^{-1} for gated (exfoliated) graphene flakes on Si/SiO_2. We note that the Landau levels in MEG structures as well as in graphene flakes floating on the graphite surface have been also visualized using tunnelling spectroscopy in magnetic fields [80, 81]. The Fermi velocity found in these later STS experiments agrees well with the magneto-transmission data in the case of MEG structures [62, 71]. The STS experiments [80] on graphene flakes on graphite indicate a surprisingly low 0.79×10^6 m s^{-1} Fermi velocity in these systems in strike difference to the value of 1.00×10^6 m s^{-1}reported from microwave absorption measurements [59]. This contradiction might be due to a different renormalization of v_F seen by these two experimental probes, or perhaps due to a very local (and invasive) character of the STM tip.

4.2.4 Beyond Simple Band Models

Relatively small but noticeable deviations of the electronic bands from their ideal linearity, on the order of a few percent at large ± 0.5 eV distances from the Dirac point, have been found by a combination of far and near-infrared magneto-optical experiments performed on multi-layer epitaxial [70]. These deviations were revealed by a departure of the observed excitations from a simple $\sqrt{B}$-dependence, which increases with the photon energy of the probing light. No signs of the electron-hole asymmetry have been found in these experiments. On the other hand, traces of the electron-hole asymmetry have been reported by Deacon et al. [68] in exfoliated graphene placed on Si/SiO_2 substrate, who estimated the difference in the electron and hole Fermi velocities to be on the order of a few percent. Magneto-transmission experiments, if carried out on neutral graphene specimens, may also bring relevant information on a conceivable appearance of a gap at the Dirac point. Working in the limit of low magnetic fields, Orlita et al. have estimated a gap to be smaller than 1 meV in quasi-neutral MEG structures [71] and its maximum possible value of a fraction of 1 meV in graphene flakes on graphite substrates [59].

4.2.5 Scattering/Disorder

Cyclotron resonance measurements on graphene, in particular in the limit of low magnetic fields (and low frequencies), can be effectively used to estimate the scattering time and/or mobility of carriers. For instance, Orlita et al. [71] (working in fields down to 10 mT range) have shown (see Fig. 4.3) the possibility to achieve a room-temperature carrier mobility exceeding 250 000 cm^2/(V s) in multi-layer epitaxial graphene, which is a record value among all other known materials. Nevertheless, the dependence of the carrier mobility on the energy, i.e., on the distance from the Dirac point, was not determined. Recent line-shape analysis of interband inter-LL resonances in equivalent specimens allowed the authors to follow

the broadening of states as a function of energy. It was shown that the mobility is a parameter strongly dependent on energy (or carrier density) in the graphene system investigated [73]. This is in contrast with the behavior typical of exfoliated graphene specimens and points towards significantly different types of scattering mechanisms in quasi-neutral epitaxial graphene, most likely due to short-range scatterers [82]. Using also magneto-optical methods, a mobility of charged carriers exceeding 10^7 cm^2/(V s) up to the temperature of liquid nitrogen has been determined for high-quality graphene flakes on the surface of bulk graphite [59]. Even today, this observations sets a surprisingly high limit for the mobility of man made structures. For this particular, natural graphene system, the energy dependence of the scattering time and or mobility has not yet been clarified.

4.2.6 Electron-Electron Interaction

Since the discovery of graphene, the effects of electron-electron interaction were a subject of particular interest in this material. Nevertheless, a great majority of experimental results obtained on various graphene systems are fairly well understood within single electron models. This also concerns a number of magneto-transmission studies [59, 62, 70, 71]. Characteristically, they display a regular, defined by a single parameter v_F, series of transitions, which are thus very tempting to be assigned as those between single particle Landau levels. However, the excitations between highly degenerate Landau levels are known as nontrivial processes which involve the effect of electron-electron interaction. The corresponding electron-hole excitation is characterized by its wave vector (which is proportional to the electron-hole separation). The specific shapes of the dispersion relations for inter and intra Landau level excitations are central for the many-body physics of the integer [5, 6, 83] and fractional [84–86] quantum Hall effects, respectively. We know from this physics that, when considering a single parabolic band of a conventional two-dimensional electron gas (with equidistant Landau levels), the energies of optically active $k = 0$ inter-Landau level excitations correspond to those of single particle excitations. This can be viewed as a consequence of Kohn's (or Larmor's) theorem and can be seen as a result of the perfect cancellation of the Coulomb binding and exchange repulsion for the $k = 0$ electron-hole excitation. This reasoning does not hold for a 2D gas of Dirac electrons, for which the exchange term may even largely exceed the Coulomb binding, and in addition be different for different pairs of Landau levels. The apparent approximate validity of the Kohn's theorem in graphene is a surprising effect, and in our opinion calls for further clarifications of the theoretical background. The first theoretical works dealing with this problem have been already published [87–89]. We note, however, that there are small (within the line width) but noticeable deviations from a perfect single particle scaling of inter Landau level excitations that have been already reported in experiments on exfoliated graphene structures [64]. Recently, Henriksen et al. [72] have reported changes in the energy of the $L_{-1(0)} \rightarrow L_{0(1)}$ transition, which is especially pronounced at high magnetic fields, when tuning the Fermi energy in between $n = -1$

and $n = 1$ Landau levels. Both these observations [64, 72] are discussed in terms of electron-electron interactions but perhaps they also include some effects of disorder [90]. Notably, magneto-optics allows for probing the nature of quasi-neutral graphene in high magnetic fields (a possible appearance of a gap in the zero LL at a filling factor of zero), which became a subject of many theoretical considerations and experimental works, see, e.g., [91, 92]. Visualization of the strong Fermi velocity enhancement [93], observed recently near the Dirac point in free-standing neutral graphene by the magneto-transport technique, is another task for infrared magneto-spectroscopy. Magneto-optical experiments performed on graphene specimens with similar quality and carrier density (decoupled graphene flakes on graphite) [59] do not show this behavior, probably as a result of strong screening effects induced by the underlying substrate.

4.2.7 Effects of Electron-Phonon Interaction

The effective coupling of optical phonons (E_{2g}) to electronic excitations in graphene yields a particularly remarkable (resonant magneto-phonon) effect when the E_{2g} phonon response is investigated as a function of the magnetic field applied across the layer [94, 95]. Then, the E_{2g} phonon is expected to hybridize with the selected $L_{n\to m}$ inter Landau level excitations. In consequence, the ample magneto-oscillations in the phonon response (in disordered systems) [79] and/or a series of avoided crossing events (in cleaner systems) [51, 96] can be observed in Raman scattering experiments. So far, an increasing number of graphene-based systems such as quasi-neutral graphene-like systems: epitaxial graphene [79], doped exfoliated graphene [97] together with the circular dichroism associated with circularly polarized phonons and a non-zero Fermi energy, in quadrilayer graphene [98], bulk graphite [52] and graphene locations on graphite surface [51, 96, 99], have shown the clear magneto-phonon resonant effect. The amplitude of this effect depends on the electron-phonon coupling constant, on the oscillator strength of the inter LL excitation, which includes matrix elements and occupation factors of the initial and final state LLs and certainly on the quality of the electronic system investigated. As for today, the most pronounced magneto-phonon effect is observed for the high quality graphene locations on a graphite substrate. This is illustrated in Fig. 4.5 with the results of recent polarization resolved magneto-Raman scattering studies of such locations on a graphite substrate. As expected from theory [94, 95] the E_{2g} phonon, observed in the σ^+/σ^- (or σ^-/σ^+) configuration of the excitation/scattered light, hybridizes with the specific asymmetric $L_{n,m}$ excitations with $|n| - |m| = \pm 1$. The appropriate analysis of the hybrid modes yields the characteristic value of $\lambda = 4.4 \times 10^{-3}$ for the electron-phonon coupling in the system investigated. Surprisingly, however, experiments show that the E_{2g} phonon of graphene on graphite couples not only with asymmetric excitations but also with other inter Landau level excitations: $L_{-n,n}$ and $L_{0,2}$. These theoretically unexpected effects remain to be clarified and could possibly be related to the particular structure of

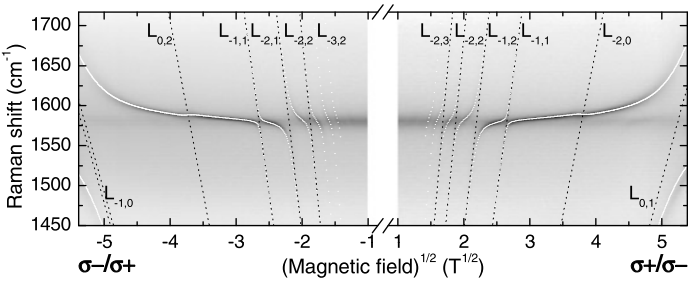

Fig. 4.5 (From Ref. [99]) Magneto-Raman scattering response: Intensity false color plot where *black* (*white*) corresponds to high (low) intensity. *Black dotted lines* are the energies of the inter-LL excitations that interact with the zone-center E_{2g}-phonon. *White lines* are the calculated hybrid electron-phonon mode energies including optical-like excitations, symmetric excitations and the $L_{0,2}$ excitation, with the parameters given on the right side. Copyright (2012) by The American Physical Society

graphene-like locations on graphite, as they were not observed in multilayer epitaxial graphene [79]. Another manifestation of electron-phonon interaction has been recently found in CR experiments on MEG structures, where a clear coupling of CR line with K point phonons has been demonstrated [100].

4.3 Magneto-Spectroscopy of Bilayer Graphene

Bernal-stacked (AB) bilayer graphene, with its nearly parabolic bands near the charge neutrality point, might provide us with a more conventional magneto-optical response as compared to graphene. Nevertheless, bilayer graphene with its zero-gap band structure and a chiral character of massive Dirac fermions carriers still exhibits a behavior that is distinctively different from other semiconducting materials.

The simplest quantum-mechanical approach to the Landau levels, originally used to interpret magneto-transport data on bilayer graphene [101], takes account of two-bands with a parabolic profile. It implies a spectrum of LLs that is linear in B [102], see Fig. 4.6a:

$$E_n = \pm\hbar\omega_c\sqrt{n(n-1)}, \quad n = 0, 1, 2, \ldots, \tag{4.2}$$

and in the limit of high n (practically even for $n > 2$), the LL spectrum (4.2) has the form $E_n \approx \pm\hbar\omega_c(n + 1/2)$, typical of conventional massive particles. The $n = 0$ and $n = 1$ levels becomes degenerate and thus form a zero-energy level with an eight-fold degeneracy and this results in a characteristic quantum Hall effect with the Berry phase of 2π [101, 102]. Dipole-allowed transitions in bilayer graphene, active in this simplest approach, follow the selection rule $|n| \rightarrow |n| \pm 1$ [69] seen in Fig. 4.6b. Raman-active modes fulfill a different set of selection rules, depending on the circular polarization of the incoming and outgoing light [54], as shown in Fig. 4.6c.

Two independent measurements have been performed up to now—on exfoliated flakes of graphene bilayer [103], and subsequently, on bilayer graphene that

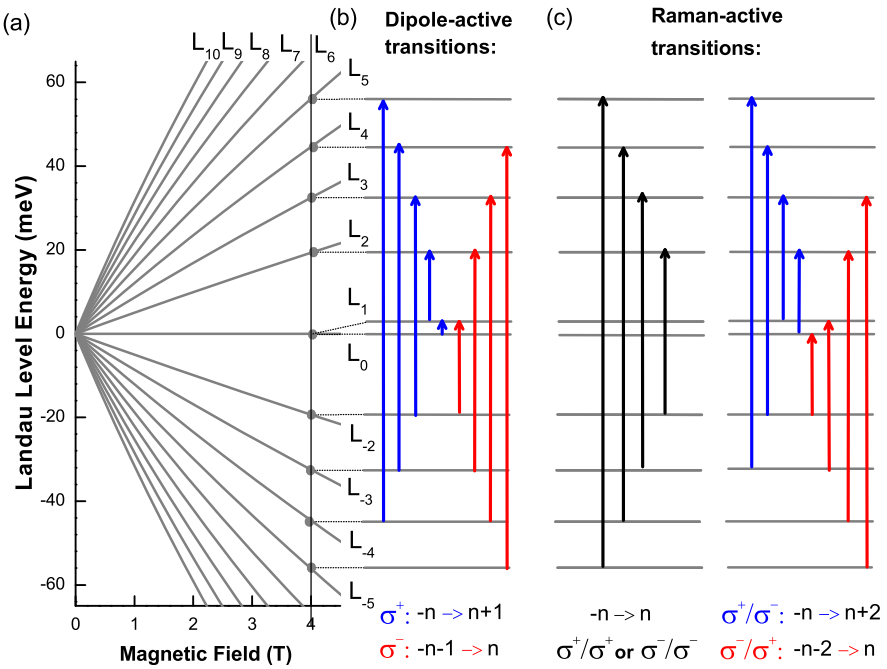

Fig. 4.6 Part (**a**): LLs in graphene bilayer, evolving nearly linearly with B at lower fields, but bending to sub-linear dependence at higher B and/or higher energies. Parts (**b**) and (**c**): Schematic plot of dipole-allowed and Raman-active inter-LL excitations in bilayer graphene

is present in a form of inclusions inside multilayer epitaxial graphene with the prevailing rotational stacking of adjacent layers [104]. The first study focuses on the intra-band response, i.e., on the cyclotron resonance of massive Dirac fermions (see Fig. 4.7a), and the second work deals with the interband inter-LL transitions (see Fig. 4.7b). In both cases, a clear departure of the optical response from a linear in B behavior has been reported, and therefore, the above theoretical model can provide a qualitative explanation only. A reasonable quantitative agreement is achieved if the LL spectrum is calculated within the four-band model. In the case of gated exfoliated flakes [72], the potential drop between layers induced by the back-gate has to be properly considered [105, 106].

Due to the lack of experimental data, a number of theoretical predictions for the magneto-optical response of bilayer graphene is still awaiting experimental verification [107–109]. These predictions involve, for instance, the appearance of the optically active transition within the zero-energy Landau level [109], corresponding to the splitting of $n = 0$ and $n = 1$ levels seen in Fig. 4.6a. Low-magnetic-field experiments in the microwave range should be a sensitive tool to study the Lifshitz transition in bilayer graphene. It is the trigonal warping, which at low energies transforms the nearly parabolic bands in bilayer graphene into four disconnected Dirac cones and changes thus significantly the topology of the band structure [69, 102, 110].

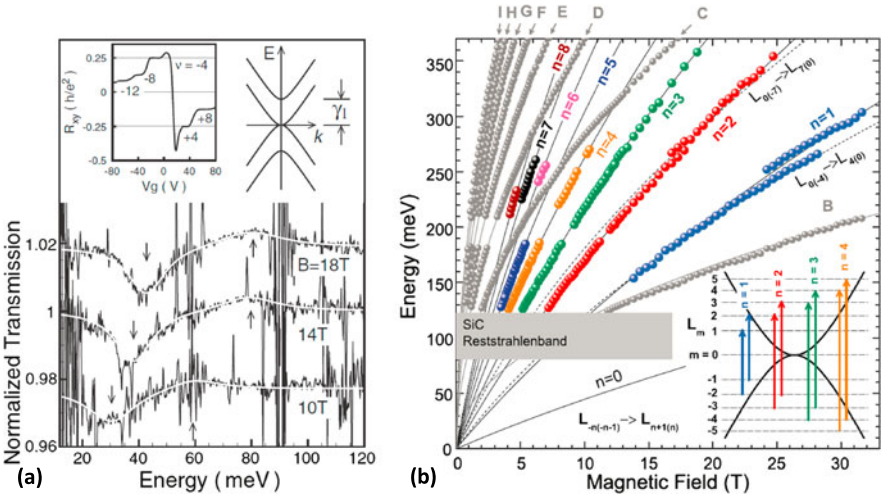

Fig. 4.7 Part (**a**): Cyclotron resonance absorption in exfoliated bilayer graphene. Taken from [103]. Copyright (2008) by The American Physical Society. Part (**b**): Fan chart of transitions observed in multi-layer epitaxial graphene. Transitions related to AB-stacked bilayer graphene inclusions are denoted by indices n and schematically depicted in the *inset*. Taken from Ref. [104]. Copyright (2011) by The American Physical Society

A new set of inter-Landau level excitations is also predicted to be active in Raman experiments [54]. Perhaps surprisingly, part of these predictions can be verified using another system, bulk graphite. As discussed in the next part, this material, namely at the K point of the band structure, shares the same single-particle Hamiltonian with bilayer graphene [111, 112].

4.4 Graphite

The renewed interest in the properties of bulk graphite is a direct consequence of the outbreak of current graphene physics. As a 3D crystal, graphite is a system characterized by a higher degree of complexity compared to graphene; nevertheless, both materials share many common properties. The appealing possibility of tracing the relativistic carriers not only in graphene monolayer and bilayer but also in bulk graphite resulted in a number of works which offer new pieces of information, new interpretations of old data, but unfortunately, often also rediscoveries of well-established prior knowledge [113].

4.4.1 Simplified Models for the Band Structure

As discussed in the preceding sections, optical spectroscopy combined with high magnetic fields can provide a unique insight into the band structure of graphene

based systems. Bulk graphite, graphene sheets in a Bernal type of stacking, is characterized by a 3D band structure defined on its 3D hexagonal Brillouin zone. A conventional description of the band structure of bulk graphite and its evolution with the magnetic field relies on the SWM model with seven $\gamma_0, \ldots, \gamma_5, \Delta$ tight binding parameters [114–116]. This model has been used to describe most of the data obtained from magneto-transport [4, 117–119], infrared magneto-reflectivity [47, 120–122], and magneto-transmission [112, 123, 124] experiments. It predicts the existence of massive electrons near the K point with a parabolic in-plane dispersion and of massless holes near the H point with a linear in-plane dispersion. Under an applied magnetic field, Landau bands are formed with a continuous dispersion along k_z, the wave vector measured in the units of the inverse inter-layer spacing, from equally spaced and linear in B Landau levels at the K point ($k_z = 0$) to non equally spaced and $\sqrt{B}$ evolving Landau levels at the H point [116] ($k_z = \pi/2$). Even though there is still no consensus concerning the precise values of the SWM parameters, mainly because of the different energy range probed in different experiments and because of the lack of polarization resolved measurements, the validity of the SWM model is generally accepted.

Instead of the full SWM model, it is often sufficient to use the effective two-parameter model [111, 125] (so-called "effective bilayer" model), which describes parabolic dispersion in the plane with the curvatures evolving along k_z. This model is obtained by (i) considering only the two first SWM parameters γ_0 and γ_1, the intra-layer and the inter-layer nearest-neighbor hopping integrals, respectively, and (ii) projecting the resulting k_z-dependent 4×4 Hamiltonian on the two low-energy bands. The Hamiltonian can be identified, at each value of k_z, to that of a graphene bilayer determined by the effective parameters γ_0 and $\gamma_1^* = 2\gamma_1 \cos k_z$. As a consequence, for $k_z = 0$ (corresponding to the K point), γ_1^* is twice enhanced with respect to γ_1 describing the real graphene bilayer. The Landau level fan chart with Landau level indices, together with dipole-allowed excitations and Raman scattering selection rules, is presented in Fig. 4.6. The electronic properties of the K point carriers in graphite are hence very similar to those of bilayer graphene.

The effective, two-parameter parabolic model has been proven to bring a fair frame to describe magneto-absorption experiments [112, 124]. It can be refined, as done in Ref. [124], by (i) introducing two different effective mass values describing positive and negative energy states, to reproduce electron-hole asymmetry, (ii) introducing a splitting of the lowest Landau level to reproduce the low energy Landau level structure of bilayer graphene and of bulk graphite. Figure 4.8a shows the results of such an analysis on magneto-absorption measurements performed on bulk graphite (from Ref. [124]). An excitation with a $\sqrt{B}$ evolution involving massless holes at the H point is observed (line A in Fig. 4.8a) together different linear in B excitations involving massive electrons at the K point. The effective two-parameter parabolic model describes most of the observed behaviors in the low magnetic field and low energy regime. Figure 4.8b shows that this model appears to be also efficient at higher values of magnetic field or of energy. It can also be used to describe few layer graphene specimens with band structures composed of superimposed graphene bilayer electronic dispersions with different values of k_z and hence of γ_1^* [111].

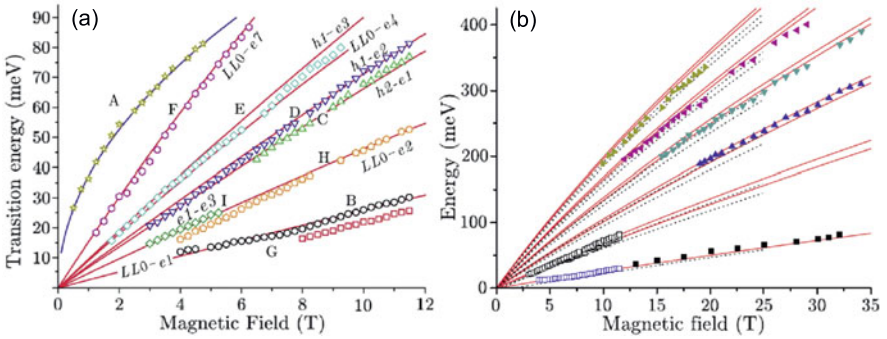

Fig. 4.8 Part (**a**): Transmission minima (*symbols*) as a function of the magnetic field. *Solid lines* are the results of the effective two-parameter model used in Ref. [124]. Part (**b**): High energy/magnetic field range with results after Ref. [112]. *Solid lines* are the same as in the *upper panel*. Adapted from Ref. [124]. Copyright (2009) by The American Physical Society

4.4.2 Full Slonczewski-Weiss-McClure Model

If polarization resolved measurements are complicated to achieve in the infrared range of energy, this problem can be overcome by using Raman scattering techniques, in the visible range of energy. Such experiments have recently been performed on bulk graphite [52]. Depending on the relative circular polarization of the excitation beam and of the scattered light, different types of electronic excitations can be selected: (i) $\Delta|n| = 0$ excitations in the co-circular polarization configurations (σ^-/σ^- and σ^+/σ^+) and (ii) $\Delta|n| = \pm 2$ and $\Delta|n| = \pm 1$ excitations in the crossed circular polarization configurations (σ^-/σ^+ and σ^+/σ^-). Strictly speaking, only $\Delta|n| = \pm 2$ excitations are expected to be Raman active, but $\Delta|n| = \pm 1$ excitations can also be observed in this polarization configuration thanks to trigonal warping. These experiments allowed us to make a direct estimation of the electron-hole asymmetry by selecting either an excitation from a level n^- to a level $(n+1)^+$ or from a level $(n+1)^-$ to n^+ for instance in the case of optical-like excitations. Figure 4.9a shows the evolution of the maxima of the scattered light as a function of the magnetic field for the two crossed circular polarization configuration together with the theoretical expectations in the frame of the full SWM model (solid and dashed lines). In contrast to the case of graphene where the main visible excitations in crossed circular polarization configuration are the $\Delta|n| = \pm 1$ excitations, the dominant contribution to the electronic Raman scattering spectrum of bulk graphite arises from $\Delta|n| = \pm 2$ electronic excitations.

Such an experiment also allowed us to probe the dispersion along k_z through the line shape of the electronic Raman scattering features, in particular those observed in both circular polarization configurations. As it is shown in Fig. 4.9b, the observed line shape is strongly asymmetric with a long tail on the high energy side of the feature. Theoretical calculations [126, 127] show that the scattered intensity, at a fixed value of the magnetic field, is directly proportional to the density of states

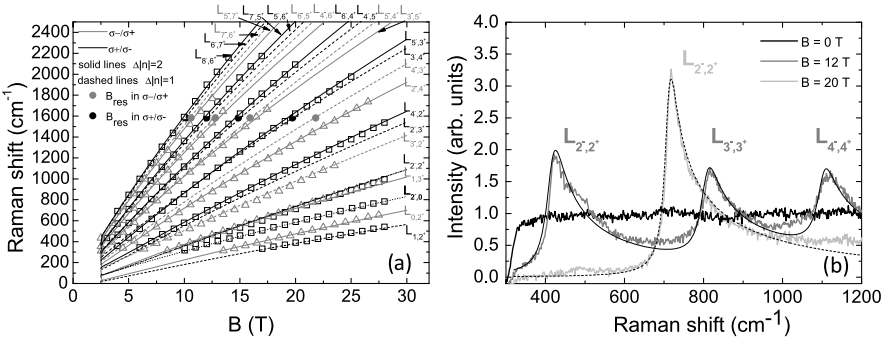

Fig. 4.9 Part (**a**): Evolution of the maxima of scattered light as a function of the magnetic field for both crossed circular polarization configurations (σ^-/σ^+ and σ^+/σ^-). *Solid* and *dashed lines* represent the expectations from the full SWM model. Part (**b**): Three Raman scattering spectra measured at $B = 0$, $B = 12$ T and $B = 20$ T in the co-circular polarization configuration (σ^-/σ^-). *Solid* and *dashed lines* are calculated line shapes. Adapted from Ref. [52]. Copyright (2011) by The American Physical Society

and one expects an energy independent response for a bilayer graphene characterized by a parabolic dispersion and a rather linear in energy response for graphene monolayer with linear dispersion. This is in striking contrast with the optical absorption which is energy independent in monolayer graphene [26] and which scales, at low energies, with the inverse of the energy for a bilayer graphene specimen [128]. Studying the K point carriers in bulk graphite with Raman scattering experiments confirms that there is a contribution of low energy electronic excitations to the Raman scattering spectrum of bulk graphite at $B = 0$, which is flat up to 1200 cm^{-1} in agreement with the expectation for a graphene bilayer, but that can be identified by applying a magnetic field. This energy independent response was also identified in unpolarized configuration [129]. Under an applied magnetic field, it then transforms into discrete features due to Landau quantization. The resulting line shape of the electronic feature observe through Raman scattering is determined mainly by the electronic dispersion around the K point and can be calculated quite accurately within the SWM model (solid and dashed lines in Fig. 4.9b). This set of experimental results can only be understood within the full SWM model taking into account the electron-hole asymmetry, the trigonal warping and the dispersion along k_z.

4.4.3 Band Structure Close to the Neutrality Point: Proximity to Lifshitz Transition

The low energy band structure of bilayer graphene and of bulk graphite, close to the charge neutrality point, is extremely sensitive to the effect of trigonal warping described by the γ_3 SWM parameter. In the case of bilayer graphene, recent magneto-transport experiments [110] performed on gated high mobility specimens, reveal that the low energy electronic dispersion is determined by interaction effects

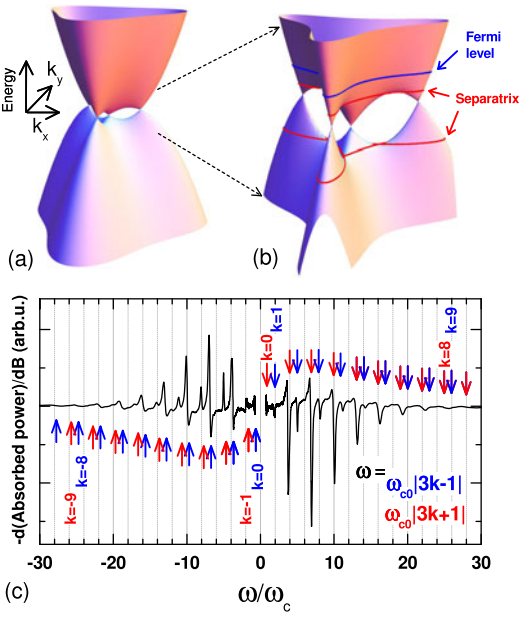

Fig. 4.10 Parts (**a**) and (**b**) Low energy in-plane band structure of bulk graphite close to the K point. *Solid red lines* show the two separatrices and the *blue solid line* shows the Fermi level. Part (**c**) Derivative of the magneto-absorption spectrum measured at a fixed microwave excitation energy of $\hbar\omega = 1.171$ meV as a function of ω/ω_c. Adapted from Ref. [130]. Copyright (2012) by The American Physical Society

which strongly modify the topology of the non trivial low energy Fermi surface. In case of ideal and noninteracting system, the electronic band structure evolves from a single electron (or hole) pocket at high energies to four distinct electron (or hole) Dirac cones when the Fermi energy is tuned to lower energies, below the topological transition named the Lifshitz transition. These magneto-transport measurements show that the low energy band structure is in fact composed of only two Dirac cones indicating a reduced symmetry caused either by the strain or, perhaps, pointing at a nematic electronic phase transition driven by a Coulomb interaction.

The band structure of bulk graphite is very similar to that of graphene bilayer, but the Fermi energy can hardly be tuned by gate effects. As a result, it is not nowadays possible to explore the situation where, as it was done for a graphene bilayer, the Fermi energy is below the separatrix. Bulk graphite is an electronic system with a Fermi energy slightly above the topological separatrices. Recent magneto-absorption experiments performed in the micro-wave range of energy (1 meV) reveal the rich physics associated with the topology of the low energy band structure close to the K point [130]. As is sketched in Fig. 4.10a and b, the band dispersion has six saddle points at two different energies ϵ_{e-sp} and ϵ_{h-sp}, which define two separatrices (iso-energetic lines separating regions with different topologies). When the Fermi energy ϵ_F crosses these separatrices, the topology of the Fermi surface changes from a single electron pocket around the K point to four disconnected cones for $\epsilon_F < \epsilon_{e\text{-}sp}$. These topological changes have a pronounced effect on the cyclotron frequency which vanishes at $\epsilon = \epsilon_{sp}$. Because ϵ_F in bulk graphite lies ~ 6 meV above ϵ_{sp}, the cyclotron resonance (CR) response measured at low energies is strongly affected. As is presented in Fig. 4.10c, which shows the derivative, with respect to magnetic field, of the magneto-absorption spectrum measured

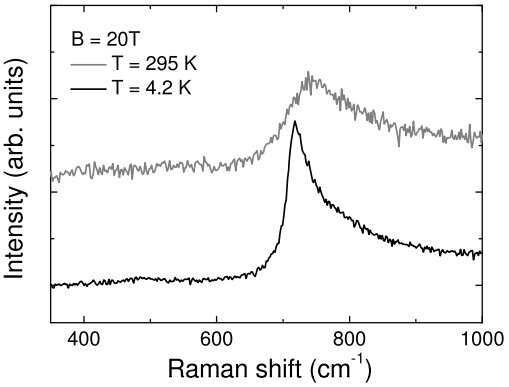

Fig. 4.11 Raman scattering spectra of the $L_{2^-,2^+}$ feature at $B = 20$ T and at $T = 4.2$ K and $T = 295$ K. Adapted from Ref. [52]. Copyright (2011) by The American Physical Society

at low temperature, this proximity results in (i) the appearance of a large number of CR harmonics (up to 20) (ii) an enhanced strength of $3k + 1$ harmonics as compared to $3k - 1$ harmonics and finally, (iii) a characteristic broadening of the observed resonances on the low energy side of the absorption peak. These are the magneto-optical signatures of the proximity to the Lifshitz transition in bulk graphite [130].

These results have been explained in the frame of a single particle model without taking interaction effects into account. Having the possibility to tune the Fermi energy across the separatrices in bulk graphite, for now, still remains a challenge.

4.4.4 Scattering Efficiency

In the case of optical excitations among discrete graphene-like Landau levels, the room temperature magneto-optical response is very similar to the one observed at low temperature, with no apparent shift nor broadening of the absorption lines [71]. This indicates that there is no relevant temperature activated scattering mechanism. The case of bulk graphite appears to be quite similar. As can be seen in Fig. 4.11, electronic Raman scattering features in a magnetic field, and in particular the $L_{2^-,2^+}$ feature, can be observed up to room temperature. The line shape of this feature is strongly affected by temperature with an overall blue shift and a smearing due to thermal population of the final state $n = 2^+$ Landau band. If the low energy onset of this feature is rather sharp at low temperature since all the $n = 2^+$ Landau band is empty down to the $k_z = 0$ states, the thermal population of this band leads to a Pauli blocking of the transitions starting from those involving the $k_z = 0$ final states. This effect quantitatively accounts for the shift and additional broadening of the $L_{2^-,2^+}$ spectrum at elevated temperatures. Thermal population effects appear to be the main source for the observed difference in the spectral response. This implies that other possible sources of spectral broadening have a negligible temperature dependence.

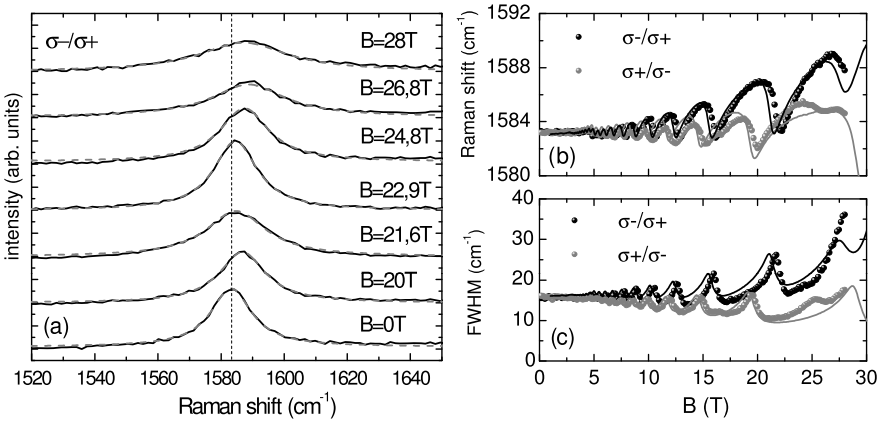

Fig. 4.12 Part (**a**) Raman scattering spectra in the E_{2g} phonon range of energy for different values of the magnetic field. Parts (**b**) and (**c**): Evolution of the Raman shift and of the FWHM of E_{2g} phonon feature as a function of the magnetic field in the two different crossed circular polarization configuration. *Solid lines* are the result of the calculation presented in Ref. [52]. Figures adapted from Ref. [52]. Copyright (2011) by The American Physical Society

4.4.5 Electron-Phonon Coupling

As in the case of graphene systems discussed in the preceding section, it is possible to tune the electron-phonon interaction to resonance in bulk graphite by applying high magnetic fields. Relevant electronic excitations for the electron-phonon coupling in bulk graphite are optical-like excitations ($\Delta k = 0$ at $B = 0$) which transform into inter Landau bands excitations with $\Delta|n| = \pm 1$ under an applied magnetic field. It is possible to tune these excitations in resonance with the E_{2g} optical phonon occurring around 1580 cm^{-1} by increasing the magnetic field. This leads to the magneto-phonon effect which manifests itself as pronounced oscillations of the phonon energy and line width, as it is shown in Fig. 4.12a. The Raman shift and the full width at half maximum (FWHM) extracted from the Lorentzian fitting of this line are presented in Fig. 4.12b and c. This effect in bulk graphite is significantly different that the one observed in the graphene monolayer. The fundamental difference between these two systems is the 3D nature of electronic states in bulk graphite and of the associated k_z dispersion. The magneto-phonon effect in bulk graphite involves Landau bands, in contrast to discrete Landau levels in graphene. The electronic dispersion close to the K point causes the oscillator strength of the optical-like excitations in this system to be spread over a significant range of energy (typically a few meV). As a result, the observed oscillations of the phonon energy and the line width are asymmetric and strongly damped, as shown in Fig. 4.12b and c. In graphene, a fully resonant coupling occurs between two discrete excitations while in bulk graphite, the 3D Landau bands that appear in magnetic field spread the interaction over a range of energy as wide as the observed electronic features. Although these oscillations are mainly due to K points excitations, they

also reflect the excitation spectrum of the H point carriers and their electron-hole asymmetry [52]. This results of the fact that the Fermi level at the H point lies below the charge neutrality point and the 0th Landau band at this particular point is completely empty. Hence, only the $L_{-1,0}$ has a finite oscillator strength and couples to the phonon while the oscillator strength of $L_{0,1}$ vanishes, creating the asymmetry observed in the two crossed circular polarization configurations, one component being blue shifted at high fields while the other component is red shifted. Modelling the magneto-phonon effect in bulk graphite allows us to extract the dimensionless electron-phonon coupling constant λ which, in this case, is 3.0×10^{-3}, approximately one third lower than the expected value. This difference probably arises from the approximation $\gamma_3 = 0$ made in the calculation which impacts the matrix elements and, *in fine*, the estimation of the coupling constant. To this end we note that in more recent, Raman scattering experiments with unpolarized light, the magneto-phonon resonance of bulk graphite could be traced in fields up to 45 T [131].

4.5 Conclusions

Concluding, the aim of our report has been to present the potential of optical magneto-spectroscopy methods to investigate the electronic properties of graphene based materials. Primarily, those methods provide the valuable information about the characteristic band structure of the system investigated. Furthermore, they also allow us to conclude on carrier scattering efficiency/mechanism and are the convenient techniques for studying the effects of electron-phonon coupling. Magneto-absorption in the far infrared range is naturally the most straightforward tool to studying the graphene and its derivatives, but this technique suffers an easy application to small size samples. A relevant step forward to applying magneto-optics to study the micron-size structure was the recent demonstration of the electronic response in magneto Raman scattering experiments. These experiments, as far performed only on graphite and on graphene locations on the graphite substrate, are certainly suitable to study all other high quality graphene structures. The fabrication of large size graphene structures (e.g., CVD growth) on one hand and a clear progress in increasing the quality (mobility) of well characterized individual graphene structures (e.g., graphene on boron nitride) on the other hand, will certainly open new possibilities for optical magneto-spectroscopy studies in a very near future. Those studies may in particular include the investigations of the effects of interactions (electron-phonon and electron-electron) in the regime of the quantum Hall effect. Other applications of optical magneto-spectroscopy might be relevant when searching for the graphene systems with an open energy gap, when studying the plasmonic structures and/or when searching for a light emission from graphene systems.

Acknowledgements The authors thank Denis Basko for stimulating discussions and acknowledge the support from the "Fondation Nanosciences" in Grenoble (DISPOGRAPH project) and the European Research Council (ERC-2012-AdG-320590-MOMB).

References

1. A.K. Geim, A.H. MacDonald, Graphene: exploring carbon flatland. Phys. Today **60**, 35–41 (2007)
2. A.K. Geim, K.S. Novoselov, The rise of graphene. Nat. Mater. **6**, 183 (2007)
3. K.S. Novoselov, A.K. Geim, S.V. Morozov, D. Jiang, M.I. Katsnelson, I.V. Grigorieva, S.V. Dubonos, A.A. Firsov, Electric field effect in atomically thin carbon films. Science **306**, 666 (2004)
4. J.A. Woollam, Spin splitting, Fermi energy changes, and anomalous g shifts in single-crystal and pyrolytic graphite. Phys. Rev. Lett. **25**, 810–813 (1970)
5. K.S. Novoselov, A.K. Geim, S.V. Morozov, D. Jiang, M.I. Katsnelson, I.V. Grigorieva, S.V. Dubonos, A.A. Firsov, Two-dimensional gas of massless Dirac fermions in graphene. Nature **438**, 197 (2005)
6. Y.B. Zhang, Y.W. Tan, H.L. Stormer, P. Kim, Experimental observation of the quantum Hall effect and Berrys phase in graphene. Nature **438**, 201 (2005)
7. M. Orlita, M. Potemski, Dirac electronic states in graphene systems: optical spectroscopy studies. Semicond. Sci. Technol. **25**, 063001 (2010)
8. F. Bonaccorso, Z. Sun, T. Hasan, A.C. Ferrari, Graphene photonics and optoelectronics. Nat. Photonics **4**, 611 (2010)
9. W.D. Tan, C.Y. Su, R.J. Knize, G.Q. Xie, L.J. Li, D.Y. Tang, Mode locking of ceramic Nd:yttrium aluminum garnet with graphene as a saturable absorber. Appl. Phys. Lett. **96**(3), 031106 (2010)
10. H. Zhang, D.Y. Tang, L.M. Zhao, Q.L. Bao, K.P. Loh, Large energy mode locking of an erbium-doped fiber laser with atomic layer graphene. Opt. Express **17**(20), 17630–17635 (2009)
11. X. Wang, L. Zhi, K. Mullen, Transparent, conductive graphene electrodes for dye-sensitized solar cells. Nano Lett. **8**(1), 323–327 (2008). PMID: 18069877
12. K.S. Kim, Y. Zhao, H. Jang, S.Y. Lee, J.M. Kim, K.S. Kim, J.-H. Ahn, P. Kim, J.-Y. Choi, B.H. Hong, Large-scale pattern growth of graphene films for stretchable transparent electrodes. Nature **457**, 706–710 (2009)
13. L. Ju, B. Geng, J. Horng, C. Girit, M. Martin, Z. Hao, H.A. Bechtel, X. Liang, A. Zettl, Y.R. Shen, F. Wang, Graphene plasmonics for tunable terahertz metamaterials. Nat. Nanotechnol. **6**, 630 (2011)
14. P. Blake, E.W. Hill, A.H. Castro Neto, K.S. Novoselov, D. Jiang, R. Yang, T.J. Booth, A.K. Geim, Making graphene visible. Appl. Phys. Lett. **91**, 063124 (2007)
15. D.S.L. Abergel, A. Russell, V.I. Fal'ko, Visibility of graphene flakes on a dielectric substrate. Appl. Phys. Lett. **91**, 063125 (2007)
16. S. Roddaro, P. Pingue, V. Piazza, V. Pellegrini, F. Beltram, The optical visibility of graphene: interference colors of ultrathin graphite on SiO_2. Nano Lett. **7**, 2707–2710 (2007)
17. C. Casiraghi, A. Hartschuh, E. Lidorikis, H. Qian, H. Harutyunyan, T. Gokus, K.S. Novoselov, A.C. Ferrari, Rayleigh imaging of graphene and graphene layers. Nano Lett. **7**, 2711–2717 (2007)
18. I. Jung, M. Pelton, R. Piner, D.A. Dikin, S. Stankovich, S. Watcharotone, M. Hausner, R.S. Ruoff, Simple approach for high-contrast optical imaging and characterization of graphene-based sheets. Nano Lett. **7**, 3569–3575 (2007)
19. A.C. Ferrari, J.C. Meyer, V. Scardaci, C. Casiraghi, M. Lazzeri, F. Mauri, S. Piscanec, D. Jiang, K.S. Novoselov, S. Roth, A.K. Geim, Raman spectrum of graphene and graphene layers. Phys. Rev. Lett. **97**, 187401 (2006)
20. D. Graf, F. Molitor, K. Ensslin, C. Stampfer, A. Jungen, C. Hierold, L. Wirtz, Spatially resolved Raman spectroscopy of single- and few-layer graphene. Nano Lett. **7**, 238–242 (2007)
21. C. Faugeras, A. Nerriere, M. Potemski, A. Mahmood, E. Dujardin, C. Berger, W.A. de Heer, Few-layer graphene on sic, pyrolitic graphite, and graphene: a Raman scattering study. Appl. Phys. Lett. **92**, 011914 (2008)

22. S. Pisana, M. Lazzeri, C. Casiraghi, K.S. Novoselov, A.K. Geim, A.C. Ferrari, F. Mauri, Breakdown of the adiabatic Born-Oppenheimer approximation in graphene. Nat. Mater. **6**, 198–201 (2007)
23. A.H. Castro Neto, F. Guinea, Electron-phonon coupling and Raman spectroscopy in graphene. Phys. Rev. B **75**, 045404 (2007)
24. J. Yan, Y. Zhang, P. Kim, A. Pinczuk, Electric field effect tuning of electron-phonon coupling in graphene. Phys. Rev. Lett. **98**, 166802 (2007)
25. T. Ando, Y. Zheng, H. Suzuura, Dynamical conductivity and zero-mode anomaly in honeycomb lattices. J. Phys. Soc. Jpn. **71**, 1318–1324 (2002)
26. R.R. Nair, P. Blake, A.N. Grigorenko, K.S. Novoselov, T.J. Booth, T. Stauber, N.M.R. Peres, A.K. Geim, Fine structure constant defines visual transparency of graphene. Science **320**, 1308 (2008)
27. K.F. Mak, M.Y. Sfeir, Y. Wu, C.H. Lui, J.A. Misewich, T.F. Heinz, Measurement of the optical conductivity of graphene. Phys. Rev. Lett. **101**, 196405 (2008)
28. A.B. Kuzmenko, E. van Heumen, F. Carbone, D. van der Marel, Universal optical conductance of graphite. Phys. Rev. Lett. **100**, 117401 (2008)
29. V.G. Kravets, A.N. Grigorenko, R.R. Nair, P. Blake, S. Anissimova, K.S. Novoselov, A.K. Geim, Spectroscopic ellipsometry of graphene and an exciton-shifted van Hove peak in absorption. Phys. Rev. B **81**, 155413 (2010)
30. K.F. Mak, J. Shan, T.F. Heinz, Seeing many-body effects in single- and few-layer graphene: observation of two-dimensional saddle-point excitons. Phys. Rev. Lett. **106**, 046401 (2011)
31. D.-H. Chae, T. Utikal, S. Weisenburger, H. Giessen, K.v. Klitzing, M. Lippitz, J. Smet, Excitonic Fano resonance in free-standing graphene. Nano Lett. **11**(3), 1379–1382 (2011)
32. S.H. Abedinpour, G. Vignale, A. Principi, M. Polini, W.-K. Tse, A.H. MacDonald, Drude weight, plasmon dispersion, and ac conductivity in doped graphene sheets. Phys. Rev. B **84**, 045429 (2011)
33. J. Horng, C.-F. Chen, B. Geng, C. Girit, Y. Zhang, Z. Hao, H.A. Bechtel, M. Martin, A. Zettl, M.F. Crommie, Y.R. Shen, F. Wang, Drude conductivity of Dirac fermions in graphene. Phys. Rev. B **83**, 165113 (2011)
34. H. Yan, F. Xia, W. Zhu, M. Freitag, C. Dimitrakopoulos, A.A. Bol, G. Tulevski, P. Avouris, Infrared spectroscopy of wafer-scale graphene. ACS Nano **5**(12), 9854–9860 (2011). doi:10.1021/nn203506n
35. M. Orlita, I. Crassee, C. Faugeras, A.B. Kuzmenko, F. Fromm, M. Ostler, T. Seyller, G. Martinez, M. Polini, M. Potemski, Classical to quantum crossover of the cyclotron resonance in graphene: a study of the strength of intraband absorption. New J. Phys. **14**(9), 095008 (2012)
36. J.M. Dawlaty, S. Shivaraman, M. Chandrashekhar, F. Rana, M.G. Spencer, Measurement of ultrafast carrier dynamics in epitaxial graphene. Appl. Phys. Lett. **92**, 042116 (2008)
37. P.A. George, J. Strait, J. Dawlaty, S. Shivaraman, M. Chandrashekhar, F. Rana, M.G. Spencer, Ultrafast optical-pump terahertz-probe spectroscopy of the carrier relaxation and recombination dynamics in epitaxial graphene. Nano Lett. **8**, 4248 (2008)
38. D. Sun, Z.-K. Wu, C. Divin, X. Li, C. Berger, W.A. de Heer, P.N. First, T.B. Norris, Ultrafast relaxation of excited Dirac fermions in epitaxial graphene using optical differential transmission spectroscopy. Phys. Rev. Lett. **101**, 157402 (2008)
39. H. Choi, F. Borondics, D.A. Siegel, S.Y. Zhou, M.C. Martin, A. Lanzara, R.A. Kaindl, Broadband electromagnetic response and ultrafast dynamics of few-layer epitaxial graphene. Appl. Phys. Lett. **94**(17), 172102 (2009)
40. P. Plochocka, P. Kossacki, A. Golnik, T. Kazimierczuk, C. Berger, W.A. de Heer, M. Potemski, Slowing hot-carrier relaxation in graphene using a magnetic field. Phys. Rev. B **80**, 245415 (2009)
41. T. Kampfrath, L. Perfetti, F. Schapper, C. Frischkorn, M. Wolf, Strongly coupled optical phonons in the ultrafast dynamics of the electronic energy and current relaxation in graphite. Phys. Rev. Lett. **95**(18), 187403 (2005)

42. M. Breusing, C. Ropers, T. Elsaesser, Ultrafast carrier dynamics in graphite. Phys. Rev. Lett. **102**, 086809 (2009)
43. R.W. Newson, J. Dean, B. Schmidt, H.M. van Driel, Ultrafast carrier kinetics in exfoliated graphene and thin graphite films. Opt. Express **17**, 2326–2333 (2009)
44. S. Winnerl, M. Orlita, P. Plochocka, P. Kossacki, M. Potemski, T. Winzer, E. Malic, A. Knorr, M. Sprinkle, C. Berger, W.A. de Heer, H. Schneider, M. Helm, Carrier relaxation in epitaxial graphene photoexcited near the Dirac point. Phys. Rev. Lett. **107**, 237401 (2011)
45. K.J. Tielrooij, J.C.W. Song, S.A. Jensen, A. Centeno, A. Pesquera, A. Zurutuza Elorza, M. Bonn, L.S. Levitov, F.H.L. Koppens, Photoexcitation cascade and multiple hot-carrier generation in graphene. Nat. Phys. **9**, 248 (2013)
46. J.K. Galt, W.A. Yager, H.W. Dail, Cyclotron resonance effects in graphite. Phys. Rev. **103**(5), 1586–1587 (1956)
47. P.R. Schroeder, M.S. Dresselhaus, A. Javan, Location of electron and hole carriers in graphite from laser magnetoreflection data. Phys. Rev. Lett. **20**, 1292 (1969)
48. T. Morimoto, Y. Hatsugai, H. Aoki, Optical Hall conductivity in ordinary and graphene quantum Hall systems. Phys. Rev. Lett. **103**, 116803 (2009)
49. I. Crassee, J. Levallois, A.L. Walter, M. Ostler, A. Bostwick, E. Rotenberg, T. Seyller, D. van der Marel, A.B. Kuzmenko, Giant Faraday rotation in single- and multilayer graphene. Nature Phys. **7**(1), 48–51 (2011)
50. R. Shimano, G. Yumoto, J.Y. Yoo, R. Matsunaga, S. Tanabe, H. Hibino, T. Morimoto, H. Aoki, Quantum Faraday and Kerr rotations in graphene. Nat. Commun. **4**, 1841 (2013)
51. C. Faugeras, M. Amado, P. Kossacki, M. Orlita, M. Kühne, A.A.L. Nicolet, Y.I. Latyshev, M. Potemski, Magneto-Raman scattering of graphene on graphite: electronic and phonon excitations. Phys. Rev. Lett. **107**, 036807 (2011)
52. P. Kossacki, C. Faugeras, M. Kuhne, M. Orlita, A.A.L. Nicolet, J.M. Schneider, D.M. Basko, Y.I. Latyshev, M. Potemski, Electronic excitations and electron-phonon coupling in bulk graphite through Raman scattering in high magnetic fields. Phys. Rev. B **84**, 235138 (2011)
53. O. Kashuba, V.I. Fal'ko, Signature of electronic excitations in the Raman spectrum of graphene. Phys. Rev. B **80**, 241404 (2009)
54. M. Mucha-Kruczyński, O. Kashuba, V.I. Fal'ko, Spectral features due to inter-Landau-level transitions in the Raman spectrum of bilayer graphene. Phys. Rev. B **82**, 045405 (2010)
55. A.M. Witowski, M. Orlita, R. Stępniewski, A. Wysmołek, J.M. Baranowski, W. Strupiński, C. Faugeras, G. Martinez, M. Potemski, Quasiclassical cyclotron resonance of Dirac fermions in highly doped graphene. Phys. Rev. B **82**, 165305 (2010)
56. I. Crassee, M. Orlita, M. Potemski, A.L. Walter, M. Ostler, T. Seyller, I. Gaponenko, J. Chen, A.B. Kuzmenko, Intrinsic terahertz plasmons and magnetoplasmons in large scale monolayer graphene. Nano Lett. **12**(5), 2470–2474 (2012)
57. H. Yan, Z. Li, X. Li, W. Zhu, P. Avouris, F. Xia, Infrared spectroscopy of tunable Dirac terahertz magneto-plasmons in graphene. Nano Lett. **12**(7), 3766–3771 (2012)
58. Y. Zheng, T. Ando, Hall conductivity of a two-dimensional graphite system. Phys. Rev. B **65**, 245420 (2002)
59. P. Neugebauer, M. Orlita, C. Faugeras, A.-L. Barra, M. Potemski, How perfect can graphene be? Phys. Rev. Lett. **103**, 136403 (2009)
60. N.M.R. Peres, F. Guinea, A.H. Castro Neto, Electronic properties of disordered two-dimensional carbon. Phys. Rev. B **73**(12), 125411 (2006)
61. V.P. Gusynin, S.G. Sharapov, Transport of Dirac quasiparticles in graphene: Hall and optical conductivities. Phys. Rev. B **73**, 245411 (2006)
62. M.L. Sadowski, G. Martinez, M. Potemski, C. Berger, W.A. de Heer, Landau level spectroscopy of ultrathin graphite layers. Phys. Rev. Lett. **97**, 266405 (2006)
63. V.P. Gusynin, S.G. Sharapov, J.P. Carbotte, Anomalous absorption line in the magneto-optical response of graphene. Phys. Rev. Lett. **98**, 157402 (2007)
64. Z. Jiang, E.A. Henriksen, L.C. Tung, Y.-J. Wang, M.E. Schwartz, M.Y. Han, P. Kim, H.L. Stormer, Infrared spectroscopy of Landau levels of graphene. Phys. Rev. Lett. **98**, 197403 (2007)

65. V.P. Gusynin, S.G. Sharapov, J.P. Carbotte, Magneto-optical conductivity in graphene. J. Phys. Condens. Matter **19**, 026222 (2007)
66. M.L. Sadowski, G. Martinez, M. Potemski, C. Berger, W.A. de Heer, Magnetospectroscopy of epitaxial few-layer graphene. Solid State Commun. **143**, 123 (2007)
67. M.L. Sadowski, G. Martinez, M. Potemski, C. Berger, W.A. de Heer, Magneto-spectroscopy of epitaxial graphene. Int. J. Mod. Phys. B **21**, 1145 (2007)
68. R.S. Deacon, K.-C. Chuang, R.J. Nicholas, K.S. Novoselov, A.K. Geim, Cyclotron resonance study of the electron and hole velocity in graphene monolayers. Phys. Rev. B **76**, 081406 (2007)
69. D.S.L. Abergel, V.I. Fal'ko, Optical and magneto-optical far-infrared properties of bilayer graphene. Phys. Rev. B **75**, 155430 (2007)
70. P. Plochocka, C. Faugeras, M. Orlita, M.L. Sadowski, G. Martinez, M. Potemski, M.O. Goerbig, J.-N. Fuchs, C. Berger, W.A. de Heer, High-energy limit of massless Dirac fermions in multilayer graphene using magneto-optical transmission spectroscopy. Phys. Rev. Lett. **100**, 087401 (2008)
71. M. Orlita, C. Faugeras, P. Plochocka, P. Neugebauer, G. Martinez, D.K. Maude, A.-L. Barra, M. Sprinkle, C. Berger, W.A. de Heer, M. Potemski, Approaching the Dirac point in high-mobility multilayer epitaxial graphene. Phys. Rev. Lett. **101**, 267601 (2008)
72. E.A. Henriksen, P. Cadden-Zimansky, Z. Jiang, Z.Q. Li, L.-C. Tung, M.E. Schwartz, M. Takita, Y.-J. Wang, P. Kim, H.L. Stormer, Interaction-induced shift of the cyclotron resonance of graphene using infrared spectroscopy. Phys. Rev. Lett. **104**, 067404 (2010)
73. M. Orlita, C. Faugeras, R. Grill, A. Wysmolek, W. Strupinski, C. Berger, W.A. de Heer, G. Martinez, M. Potemski, Carrier scattering from dynamical magnetoconductivity in quasineutral epitaxial graphene. Phys. Rev. Lett. **107**, 216603 (2011)
74. M. Schultz, U. Merkt, A. Sonntag, U. Rossler, Density dependent cyclotron and intersubband resonance in inverted CdTe/HgTe/CdTe quantum wells. J. Cryst. Growth **184–185**, 1180 (1998)
75. M. Schultz, U. Merkt, A. Sonntag, U. Rossler, R. Winkler, T. Colin, P. Helgesen, T. Skauli, S. Løvold, Crossing of conduction- and valence-subband Landau levels in an inverted HgTe/CdTe quantum well. Phys. Rev. B **57**, 14772 (1998)
76. M. Orlita, K. Masztalerz, C. Faugeras, M. Potemski, E.G. Novik, C. Brüne, H. Buhmann, L.W. Molenkamp, Fine structure of zero-mode Landau levels in HgTe/Hg_xCd_{1-x}Te quantum wells. Phys. Rev. B **83**, 115307 (2011)
77. M. Zholudev, F. Teppe, M. Orlita, C. Consejo, J. Torres, N. Dyakonova, M. Czapkiewicz, J. Wróbel, G. Grabecki, N. Mikhailov, S. Dvoretskii, A. Ikonnikov, K. Spirin, V. Aleshkin, V. Gavrilenko, W. Knap, Magnetospectroscopy of two-dimensional HgTe-based topological insulators around the critical thickness. Phys. Rev. B **86**, 205420 (2012)
78. H. Farhat, S. Berciaud, M. Kalbac, R. Saito, T.F. Heinz, M.S. Dresselhaus, J. Kong, Observation of electronic Raman scattering in metallic carbon nanotubes. Phys. Rev. Lett. **107**, 157401 (2011)
79. C. Faugeras, M. Amado, P. Kossacki, M. Orlita, M. Sprinkle, C. Berger, W.A. de Heer, M. Potemski, Tuning the electron-phonon coupling in multilayer graphene with magnetic fields. Phys. Rev. Lett. **103**, 186803 (2009)
80. G. Li, A. Luican, E.Y. Andrei, Scanning tunneling spectroscopy of graphene on graphite. Phys. Rev. Lett. **102**, 176804 (2009)
81. D.L. Miller, K.D. Kubista, G.M. Rutter, M. Ruan, W.A. de Heer, P.N. First, J.A. Stroscio, Observing the quantization of zero mass carriers in graphene. Science **324**, 924–927 (2009)
82. N.H. Shon, T. Ando, Quantum transport in two-dimensional graphite system. J. Phys. Soc. Jpn. **67**, 2421 (1998)
83. K.V. Klitzing, G. Dorda, M. Pepper, New method for high-accuracy determination of the fine-structure constant based on quantized Hall resistance. Phys. Rev. Lett. **45**, 494–497 (1980)
84. D.C. Tsui, H.L. Stormer, A.C. Gossard, Two-dimensional magnetotransport in the extreme quantum limit. Phys. Rev. Lett. **48**, 1559–1562 (1982)

85. X. Du, I. Skachko, F. Duerr, A. Luican, E.Y. Andrei, Fractional quantum Hall effect and insulating phase of Dirac electrons in graphene. Nature **462**, 192 (2009)
86. K.I. Bolotin, F. Ghahari, M.D. Shulman, H.L. Stormer, P. Kim, Observation of the fractional quantum Hall effect in graphene. Nature **462**, 196 (2009)
87. A. Iyengar, J. Wang, H.A. Fertig, L. Brey, Excitations from filled Landau levels in graphene. Phys. Rev. B **75**, 125430 (2007)
88. Y.A. Bychkov, G. Martinez, Magnetoplasmon excitations in graphene for filling factors $\nu \leq 6$. Phys. Rev. B **77**, 125417 (2008)
89. K. Asano, T. Ando, Approximate validity of Kohn's theorem in graphene. Work Presented at EP2DS-18 Conference, Japan, 2009
90. W. Zhu, Q.W. Shi, J.G. Hou, X.R. Wang, Comment on "interaction-induced shift of the cyclotron resonance of graphene using infrared spectroscopy". Phys. Rev. Lett. **105**, 159703 (2010)
91. M.I. Katsnelson, Graphene: carbon in two dimensions. Mater. Today **10**, 20–27 (2007)
92. A.J.M. Giesbers, U. Zeitler, M.I. Katsnelson, L.A. Ponomarenko, T.M. Mohiuddin, J.C. Maan, Quantum-Hall activation gaps in graphene. Phys. Rev. Lett. **99**, 206803 (2007)
93. D.C. Elias, R.V. Gorbachev, A.S. Mayorov, S.V. Morozov, A.A. Zhukov, P. Blake, L.A. Ponomarenko, I.V. Grigorieva, K.S. Novoselov, F. Guinea, A.K. Geim, Dirac cones reshaped by interaction effects in suspended graphene. Nat. Phys. **7**, 701 (2011)
94. T. Ando, Magnetic oscillation of optical phonon in graphene. J. Phys. Soc. Jpn. **76**, 024712 (2007)
95. M.O. Goerbig, J.-N. Fuchs, K. Kechedzhi, V.I. Fal'ko, Filling-factor-dependent magnetophonon resonance in graphene. Phys. Rev. Lett. **99**, 087402 (2007)
96. J. Yan, S. Goler, T.D. Rhone, M. Han, R. He, P. Kim, V. Pellegrini, A. Pinczuk, Observation of magnetophonon resonance of Dirac fermions in graphite. Phys. Rev. Lett. **105**, 227401 (2010)
97. P. Kossacki, C. Faugeras, M. Kuhne, M. Orlita, A. Mahmood, E. Dujardin, R.R. Nair, A.K. Geim, M. Potemski, Circular dichroism of magneto-phonon resonance in doped graphene. Phys. Rev. B **86**, 205431 (2012)
98. C. Faugeras, P. Kossacki, A.A.L. Nicolet, M. Orlita, M. Potemski, A. Mahmood, D.M. Basko, Probing the band structure of quadrilayer graphene with magneto-phonon resonance. New J. Phys. **14**, 095007 (2012)
99. M. Kühne, C. Faugeras, P. Kossacki, A.A.L. Nicolet, M. Orlita, Y.I. Latyshev, M. Potemski, Polarization-resolved magneto-Raman scattering of graphenelike domains on natural graphite. Phys. Rev. B **85**, 195406 (2012)
100. M. Orlita, L.Z. Tan, M. Potemski, M. Sprinkle, C. Berger, W.A. de Heer, S.G. Louie, G. Martinez, Resonant excitation of graphene k-phonon and intra-Landau-level excitons in magneto-optical spectroscopy. Phys. Rev. Lett. **108**, 247401 (2012)
101. K.S. Novoselov, E. McCann, S.V. Morozov, V.I. Fal'ko, K.I. Katsnelson, U. Zeitler, D. Jiang, F. Schedin, A.K. Geim, Unconventional quantum Hall effect and Berry's phase of 2π in bilayer graphene. Nat. Phys. **2**, 177–180 (2006)
102. E. McCann, V.I. Fal'ko, Landau-level degeneracy and quantum Hall effect in a graphite bilayer. Phys. Rev. Lett. **96**, 086805 (2006)
103. E.A. Henriksen, Z. Jiang, L.-C. Tung, M.E. Schwartz, M. Takita, Y.-J. Wang, P. Kim, H.L. Stormer, Cyclotron resonance in bilayer graphene. Phys. Rev. Lett. **100**, 087403 (2008)
104. M. Orlita, C. Faugeras, J. Borysiuk, J.M. Baranowski, W. Strupiński, M. Sprinkle, C. Berger, W.A. de Heer, D.M. Basko, G. Martinez, M. Potemski, Magneto-optics of bilayer inclusions in multilayered epitaxial graphene on the carbon face of sic. Phys. Rev. B **83**, 125302 (2011)
105. M. Mucha-Kruczynski, E. McCann, V.I. Fal'ko, The influence of interlayer asymmetry on the magnetospectroscopy of bilayer graphene. Solid State Commun. **149**, 1111–1116 (2009)
106. M. Mucha-Kruczynski, D.S.L. Abergel, E. McCann, V.I. Fal'ko, On spectral properties of bilayer graphene: the effect of an sic substrate and infrared magneto-spectroscopy. J. Phys. Condens. Matter **21**, 344206 (2009)

107. C. Töke, V.I. Falko, Intra-Landau-level magnetoexcitons and the transition between quantum Hall states in undoped bilayer graphene. Phys. Rev. B **83**, 115455 (2011)
108. V.E. Bisti, N.N. Kirova, Coulomb interaction and electron-hole asymmetry in cyclotron resonance of bilayer graphene in a high magnetic field. Phys. Rev. B **84**, 155434 (2011)
109. Y. Barlas, R. Côté, K. Nomura, A.H. MacDonald, Intra-Landau-level cyclotron resonance in bilayer graphene. Phys. Rev. Lett. **101**, 097601 (2008)
110. A.S. Mayorov, D.C. Elias, M. Mucha-Kruczynski, R.V. Gorbachev, T. Tudorovskiy, A. Zhukov, S.V. Morozov, M.I. Katsnelson, V.I. Falko, A.K. Geim, K.S. Novoselov, Interaction-driven spectrum reconstruction in bilayer graphene. Science **333**(6044), 860–863 (2011)
111. M. Koshino, T. Ando, Magneto-optical properties of multilayer graphene. Phys. Rev. B **77**, 115313 (2008)
112. M. Orlita, C. Faugeras, J.M. Schneider, G. Martinez, D.K. Maude, M. Potemski, Graphite from the viewpoint of Landau level spectroscopy: an effective graphene bilayer and monolayer. Phys. Rev. Lett. **102**, 166401 (2009)
113. N.B. Brandt, S.M. Chudinov, Y.G. Ponomarev, *Semimetals 1: Graphite and Its Compounds*. Modern Problems in Condensed Matter Sciences, vol. 20.1 (North-Holland, Amsterdam, 1988)
114. J.C. Slonczewski, P.R. Weiss, Band structure of graphite. Phys. Rev. **109**, 272 (1958)
115. J.W. McClure, Diamagnetism of graphite. Phys. Rev. **104**, 666–671 (1956)
116. K. Nakao, Landau level structure and magnetic breakthrough in graphite. J. Phys. Soc. Jpn. **40**, 761 (1976)
117. D.E. Soule, Magnetic field dependence of the Hall effect and magnetoresistance in graphite single crystals. Phys. Rev. **112**, 698–707 (1958)
118. D.E. Soule, J.W. McClure, L.B. Smith, Study of the Shubnikov-de Haas effect. Determination of the Fermi surfaces in graphite. Phys. Rev. **134**, 453–470 (1964)
119. J.M. Schneider, M. Orlita, M. Potemski, D.K. Maude, Consistent interpretation of the low-temperature magnetotransport in graphite using the Slonczewski-Weiss-McClure 3D band-structure calculations. Phys. Rev. Lett. **102**, 166403 (2009)
120. W.W. Toy, M.S. Dresselhaus, G. Dresselhaus, Minority carriers in graphite and the h-point magnetoreflection spectra. Phys. Rev. B **15**, 4077 (1977)
121. Z.Q. Li, S.-W. Tsai, W.J. Padilla, S.V. Dordevic, K.S. Burch, Y.J. Wang, D.N. Basov, Infrared probe of the anomalous magnetotransport of highly oriented pyrolytic graphite in the extreme quantum limit. Phys. Rev. B **74**, 195404 (2006)
122. J. Levallois, M. Tran, A.B. Kuzmenko, Decrypting the cyclotron effect in graphite using Kerr rotation spectroscopy. Solid State Commun. **152**(15), 1294–1300 (2012)
123. M. Orlita, C. Faugeras, G. Martinez, D.K. Maude, M.L. Sadowski, M. Potemski, Dirac fermions at the h point of graphite: magnetotransmission studies. Phys. Rev. Lett. **100**, 136403 (2008)
124. K.-C. Chuang, A.M.R. Baker, R.J. Nicholas, Magnetoabsorption study of Landau levels in graphite. Phys. Rev. B **80**, 161410 (2009)
125. B. Partoens, F.M. Peeters, Normal and Dirac fermions in graphene multilayers: tight-binding description of the electronic structure. Phys. Rev. B **75**, 193402 (2007)
126. O. Kashuba, V.I. Fal'ko, Signature of electronic excitations in the Raman spectrum of graphene. Phys. Rev. B **80**, 241404 (2009)
127. M. Mucha-Kruczynski, O. Kashuba, V.I. Fal'ko, Spectral features due to inter-Landau-level transitions in the Raman spectrum of bilayer graphene. Phys. Rev. B **82**, 045405 (2010)
128. E. McCann, D.S.L. Abergel, V.I. Falko, Electrons in bilayer graphene. Solid State Commun. **146**, 110 (2007)
129. A.F. García-Flores, H. Terashita, E. Granado, Y. Kopelevich, Landau levels in bulk graphite by Raman spectroscopy. Phys. Rev. B **79**, 113105 (2009)

130. M. Orlita, P. Neugebauer, C. Faugeras, A.-L. Barra, M. Potemski, F.M.D. Pellegrino, D.M. Basko, Cyclotron motion in the vicinity of a Lifshitz transition in graphite. Phys. Rev. Lett. **108**, 017602 (2012)
131. Y. Kim, Y. Ma, A. Imambekov, N.G. Kalugin, A. Lombardo, A.C. Ferrari, J. Kono, D. Smirnov, Magnetophonon resonance in graphite: high-field Raman measurements and electron-phonon coupling contributions. Phys. Rev. B **85**, 121403 (2012)